Research Square

Preprints are preliminary reports that have not undergone peer review.
They should not be considered conclusive, used to inform clinical practice,
or referenced by the media as validated information.

An integrated assessment of seismic hazard exposure and its societal impact in Seven Sister States of North Eastern Region of India for sustainable disaster mitigation planning

Navdeep Agrawal
Shiv Nadar University
Laxmi Gupta
Shiv Nadar University
Jagabandhu Dixit (jagabandhu.dixit@snu.edu.in)
Shiv Nadar University https://orcid.org/0000-0002-5450-578X
Sujit Kumar Dash
Indian Institute of Technology Kharagpur

Research Article

Keywords: North East India, seismic hazard, social vulnerability index, cluster analysis, seismic exposure

Posted Date: October 21st, 2021

DOI: https://doi.org/10.21203/rs.3.rs-1003515/v1

License: This work is licensed under a Creative Commons Attribution 4.0 International License.
Read Full License

An integrated assessment of seismic hazard exposure and its societal impact in Seven Sister States of North Eastern Region of India for sustainable disaster mitigation planning

Navdeep Agrawal[1], Laxmi Gupta[1], Jagabandhu Dixit[1,*], Sujit Kumar Dash[2]

[1]Disaster Management Laboratory, Shiv Nadar University, Delhi NCR, Greater Noida, Uttar Pradesh 201314, India.

[2]Department of Civil Engineering, Indian Institute of Technology Kharagpur, Kharagpur, West Bengal 721302, India.

E-mail address of authors: na655@snu.edu.in; lg100@snu.edu.in; sujit@civil.iitkgp.ac.in

***Corresponding Author**: Jagabandhu Dixit, Email: jagabandhu.dixit@snu.edu.in

Abstract

The Seven Sister States of the North Eastern Region of India, located on the complex seismotectonic belt, is characterized by high seismicity. A comprehensive seismic hazard exposure assessment is carried out by quantifying hazard using a probabilistic approach, vulnerability by factor analysis, and exposure mapping by integrating seismic hazard and vulnerability. Peak ground acceleration (PGA) values at bedrock are calculated with the help of ground motion prediction equations (GMPE) for 10% probability of exceedance in 50 years (475 years) and 100 years (950 years), and 2% probability of exceedance in 50 years (2475 years). The resulting spatial distribution of the PGA values considering return periods of 475, 950, and 2475 years are presented through seismic hazard maps. The social vulnerability analysis indicates that 21 districts covering 91.43% area of the state of Assam and the entire state of Tripura are under high vulnerability. With the help of spatial cluster analysis, it is found

that 17.14% of the study area are having an average social vulnerability index (SVI) score of 0.329 and therefore can be considered as hotspots. Through seismic hazard analysis, it is observed that more than 50% of the area of North East India is under moderate to very high exposure class. The seismic hazard maps developed can help in disaster mitigation planning and execution leading to sustainable development goals and targets.

Keywords: North East India, seismic hazard, social vulnerability index, cluster analysis, seismic exposure

1. Introduction

The North Eastern Region (NER) of India comprises eight states, namely Arunachal Pradesh, Assam, Manipur, Meghalaya, Mizoram, Nagaland, Tripura, and Sikkim. The Seven Sister States (SSS) of India is a popular term for the seven contiguous states in NER except for Sikkim. The Himalayan arc ranges, extending from west-northwest to east-southeast of India, lies near the subduction zone of Indian and Eurasian tectonic plates. Due to the collision of the Indian plate with the Tibet plateau towards the northern part and the Burmese landmass towards the east, the formation of seismotectonic features like the Himalayan thrust, Arakan-Yoma, Naga Hills, and Tripura fold have resulted (Verma and Kumar 1987). The Himalayan tectonic feature in north-eastern India is very complex and exhibits high seismicity. Due to its geological, geomorphological, and seismotectonic setting, the NER is highly exposed to seismic hazards. The region has suffered extensive loss of lives and damage to property due to significant earthquakes in the past. On 28 April 2021, an M_w 6.0 earthquake occurred near Dhekiajuli in Assam, India, leading to ground cracking and the collapse of several houses. For the past few decades, The NER has been experiencing high seismic risk, which can be attributed to an increase in population density and unplanned rapid urbanization and infrastructure developments.

Quantifying seismic risk by assessment of hazard and vulnerability at a regional level is a significant step towards effective disaster risk reduction and mitigation strategies. Seismic hazard deals with the quantification of ground motion at a particular site in a specific time interval which can be expressed in terms of peak ground acceleration (PGA) or spectral acceleration (SA), or any other ground motion parameter (GMP) (Kramer 1996). The vulnerability could be either social or physical. However, it is primarily defined by the social, economic, natural, and built environmental conditions of a community that affects its susceptibility towards the hazards significantly (Cutter et al. 2008). The physical vulnerability deals with the building stock in the vicinity and their susceptibility to hazard. In contrast, social vulnerability is concerned with identifying vulnerable groups of the society in the region and the factors that can affect it directly or indirectly (Cutter 1996). Therefore, the combined study of seismic hazard and social vulnerability will enable the policymakers, urban planners, and other concerned authorities to pre-identify the localities prone to high potential seismic hazards. Moreover, such a study shall help in understanding the impact of the seismic hazard on the lives of the people living in the vicinity of such disaster-prone areas.

In the past, many researchers like Sharma and Malik (2006), Raghukanth and Dash (2010), NDMA (2010), Raghukanth et al. (2011), Nath and Thingbaijam (2012), Das et al. (2016), Dixit et al. (2016), and Ghione et al. (2021) have contributed to different aspects of seismic risk assessment for the NER of India with a common goal to reduce the disaster risk. At the regional level, such seismic hazard studies are also available, Sitharam and Sil (2014) for the state of Tripura and Mizoram; Baro et al. (2018) for the Shillong Plateau, Meghalaya; Bahuguna; and Sil (2020) for the state of Assam. However, these studies have only focused on the seismic hazard assessment, either deterministically (DSHA) or probabilistically (PSHA), but have not considered the vulnerability aspect which is an equally important issue. Worldwide, several studies have been conducted on social vulnerability in regards to seismic

hazard by considering different assessment frameworks like the Hazard of Place Model, HoP (Cutter 1996), the BBC model (Brikmann 2013), Disaster of Resilience of Place model, DROP (Cutter et al. 2008), and methods like multicriteria analysis, MCA (Martins et al. 2012; Frigerio et al. 2016; Armas and Gavris 2017; Derakhshan et al. 2020; and Agrawal et al. 2021). In the Indian scenario, most seismic hazard vulnerability studies are directed towards the built environment (Sarmah and Das 2018; Dutta, Halder, and Sharma 2021). For NER, social vulnerability assessment (SVA) due to climate change and environmental hazards were performed by Maiti et al. (2017) and Das et al. (2021), respectively. However, social vulnerability studies of the NER due to seismic hazards are very limited. This is primarily because such studies involve diverse seismic and demographic databases which are relatively difficult to obtain. The present study has investigated this issue through probabilistic seismic hazard analysis and social vulnerability studies.

The objective of the present study is to develop the updated seismic hazard map of the Seven Sister States of northeast India using PSHA based on the updated earthquake catalogue and conduct social vulnerability assessment and exposure to seismic hazard. A circle of radius 500 km (around 26.16°N and 93.28°E) covering the entire NER is constructed for the development of the seismotectonic model, and the region is segmented into 0.2° x 0.2° grids (Anbazhagan et al. 2019). Following the PSHA approach, the seismic hazard is assessed at the center of each grid. The data obtained is then utilized to quantify the PGA values at the bedrock level for 10% probability of exceedance in 50 and 100 years and 2% probability of exceedance in 50 years. Subsequently, the PGA values are plotted in the GIS environment leading to seismic hazard maps.

For SVA, the indicators are selected by the application of principal component analysis (PCA) and factor analysis (FA) within the framework of the HoP model for the generation of the social vulnerability index, SVI (Agrawal et al. 2021). Additionally, with the help of spatial statistical

and cluster analysis tools in the GIS environment, hotspot and cold spot clusters within the study area are identified. Finally, the seismic hazard map is integrated with the SVI, and exposure maps for the NER are developed.

2. Study Area

The present study area consists of the Seven Sister States (SSS) of northeast India, namely, Arunachal Pradesh, Assam, Manipur, Meghalaya, Mizoram, Nagaland, and Tripura. It lies between 20°N-30°N latitude and 87°E-98°E longitude (Fig. 1). Geographically, it can be classified into the Eastern Himalayas, Barak valley, Patkai hills, and Brahmaputra valley plains (Verma 2018).

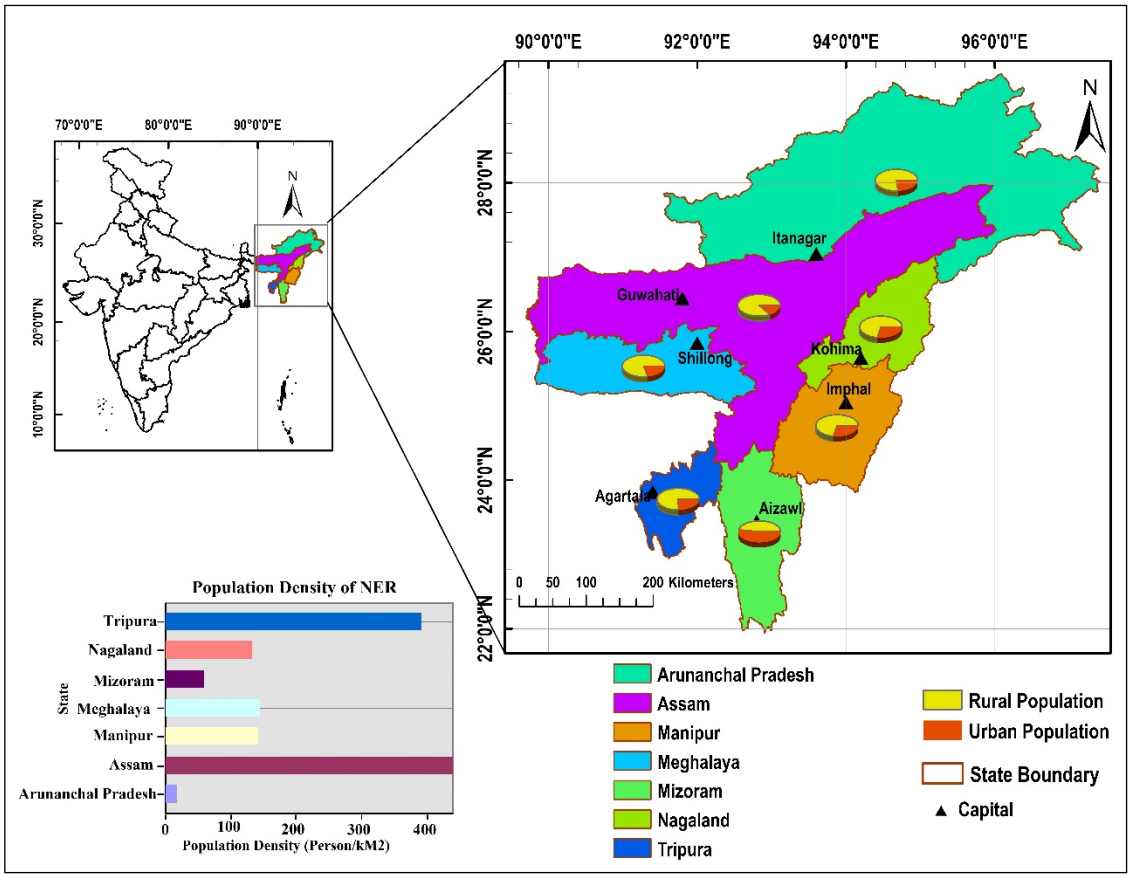

Fig. 1 Study area: Seven Sister States in NER of India

The presence of the Indo-Burmese plate boundary in the eastern region and the Indo-Eurasian plate boundary in the northern region (Baro et al. 2018), makes the NER one of the most seismically active regions in the world. As per IS1893 (2016), it is categorized as the most

severe seismic zone in India i.e. zone V. Its tectonic setting is shown in Fig. 2. In the past, several high-intensity earthquakes such as the 1869 Cachar earthquake, 1897 Shillong earthquake, 1918 Meghalaya earthquake, 1947 Arunachal Pradesh earthquake, and 1950 Assam earthquake; have severely affected this region.

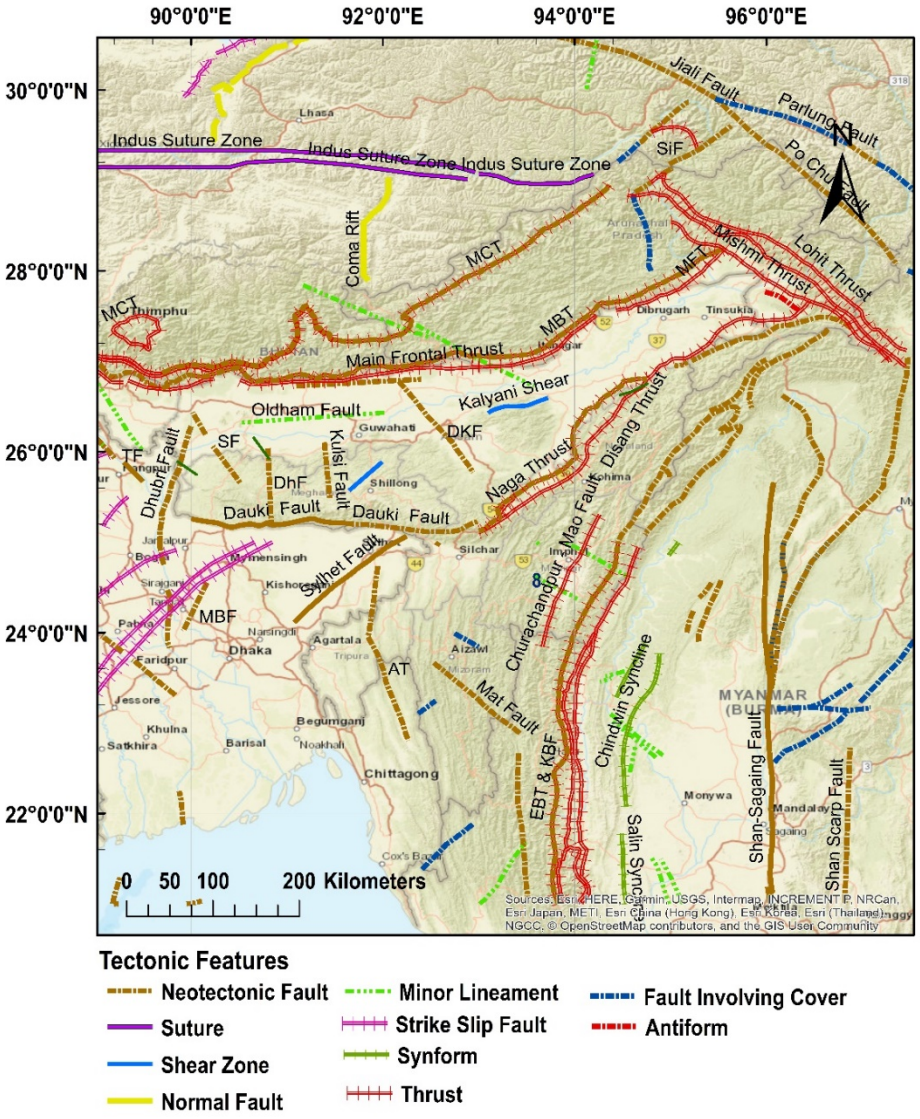

Fig. 2 Seismotectonic features of NER of India

In all states of the SSS, except Mizoram, more than 70% population live in rural areas (Census 2011). The primary source of their economy is agriculture. This is because due to inaccessible terrain and lack of transportation networks, few industries have developed in this region. High population density is observed in the states of Assam and Tripura with 439.43 and 389.11

people per sq. km, respectively, which is possibly due to the presence of better employment opportunities. In Arunachal Pradesh and Mizoram, the population density is the lowest i.e. 17.26, 58.90 people per sq. km, respectively (Fig.1). The population of Assam constitutes more than 65% of the total population of the SSS region (Census 2011). High population growth, increased infrastructure, unplanned urbanization, and complex seismotectonic regime tends to increase the seismic risk of this region. Therefore, a comprehensive seismic hazard analysis and social vulnerability assessment at the regional level is highly essential for effective disaster risk management leading to the reduction of loss of lives and property.

3. Methodology

The present study consists of (a) seismic hazard assessment, (b) social vulnerability assessment, and (c) quantification of exposure to the seismic hazard; details of which are presented below.

3.1 *Seismic Hazard Assessment (SHA)*

The probabilistic approach (PSHA), adopted in the present study, can effectively consider the uncertainties in the earthquake magnitude, location, and time of occurrence, etc. Like DSHA, PSHA does not focus on an exclusive event for worst-case scenarios; instead, it contemplates all possible earthquakes from all potential seismic sources. For PSHA, seismicity of each source zone, uncertainties in location, size, and ground motion to obtain the probability that a GMP will be exceeded during a particular period is taken into account (Kramer 1996).

3.1.1 *Data Acquisition*

The earthquake catalogue for the NER is compiled over an area of radius of 500 km, centered around the coordinate point of 26.16°N and 93.28°E. The details of 8959 earthquake events from 1760 to 2021 (261 years) were obtained from the databases like the National Center for Seismology (NCS), India, Bhukosh-Geological Survey of India, United States Geological

Survey (USGS), and International Seismological Center (ISC), etc. The compiled catalogue comprises events in different magnitude scales, like body-wave magnitude (m_b), surface-wave magnitude (M_S), local magnitude (M_L), and moment magnitude scale (M_w). For a rational seismic hazard analysis, a uniform magnitude scale is necessary the details of which are explained below.

3.1.2 *Homogenization and Declustering*

The earthquake catalogue is homogenized to a common magnitude scale (i.e., M_w) using an orthogonal regression approach (Wason et al. 2012). There are 349, 277, and 130 data points for the orthogonal regression between m_b and M_w, M_L and M_w, and M_S and M_w, respectively (Fig 3). The newly developed region-specific regression relation between moment magnitude (M_w) and other magnitude scales for the NER are shown in Table 1.

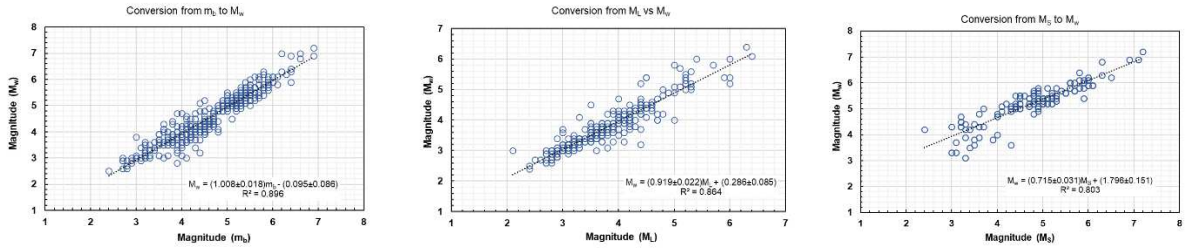

(a) (b) (c)

Fig. 3 Conversion from (a) m_b to M_w, (b) M_L to M_w, and (c) M_S to M_w

Table 1 Relation between different magnitude scales

Scale	data points	Relation		R^2
m_b to M_w	349	$M_w = (1.008\pm0.018)\, m_b - (0.095\pm0.086)$	$2.4 \leq m_b \leq 6.9$	0.896
M_L to M_w	277	$M_w = (0.919\pm0.022)\, M_L + (0.286\pm0.085)$	$2.5 \leq M_L \leq 7.0$	0.864
M_S to M_w	130	$M_w = (0.715\pm0.031)\, M_S + (1.796\pm0.151)$	$3.0 \leq M_S \leq 7.2$	0.803

From the unified earthquake catalogue, the foreshocks and aftershocks are removed by declustering as they are dependent on the mainshock, spatially and temporally (Zhuang, Ogata and Vere-Jones 2002). In this study, an open-source software ZMAP (v7.0) by Wiemer (2001) is utilized to eliminate the dependent events by following the methodology proposed by Gardner and Knopoff (1974) which follows a Poisson distribution (Stiphout et al. 2012). A similar procedure has been followed by Sitharam and Sil (2014), and Anbazhagan et al. 2019.

After declustering, it was found that 26.34% of the events are interdependent and, therefore, were eliminated from the data set. Consequently, only 6599 events are retained in the dataset, among which 4837 events are greater than M_w 3.5.

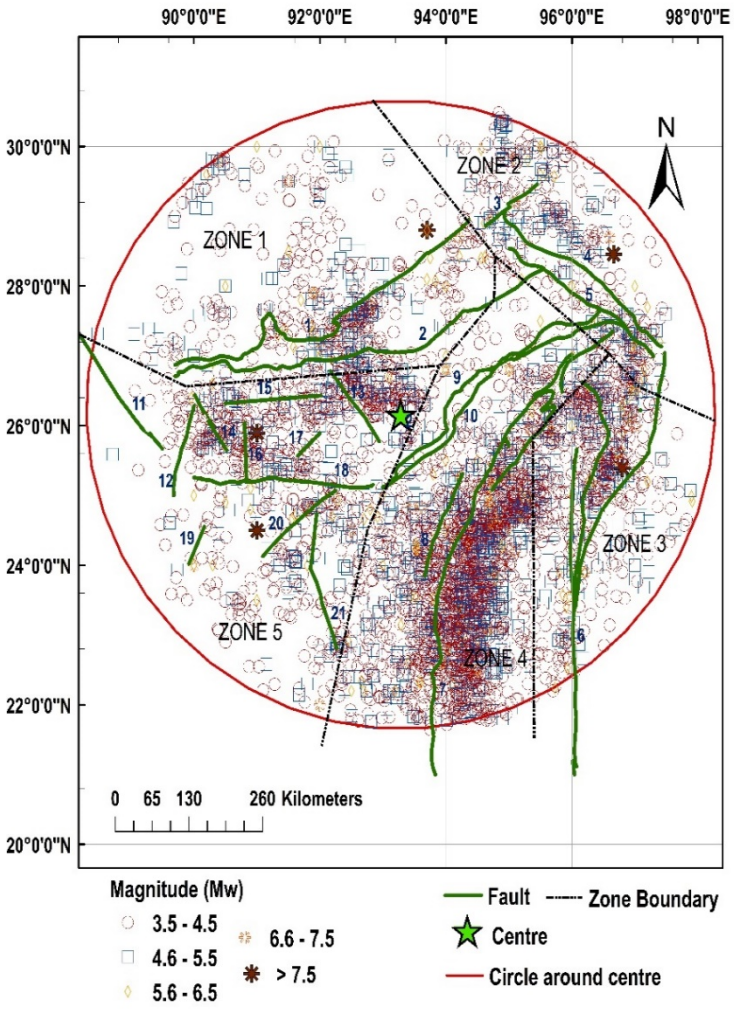

Fig. 4 Seismic source zone demarcation with major faults and declustered-homogenized earthquake

3.1.3 *Seismic Source Zonation*

Seismic source zonation is considered an essential pre-requirement for the seismic hazard study. In the present study, the study area is divided into five source zones that are distinct in terms of fault properties, seismic source, geology, and plate tectonics (Fig. 4).

3.1.4 *Completeness of Catalogue*

For PSHA, it is also necessary to check for completeness of the data in terms of magnitude and time. The magnitude of completeness (*Mc*) is the lowest magnitude above which the catalogue, in a selected space-time window, is considered to be complete (Rydelek and Sacks 1989; Wiemer and Wyss 2000). M_C, in the present study, is obtained through the maximum curvature method (MAXC). A similar procedure has been adopted by various scholars worldwide (Woessner and Wiemer 2005). The open-source software ZMAP (v 7.0) by Wiemer (2001) was used for this purpose and the obtained values of the M_C are presented in Table 2.

The completeness study of seismic data in terms of time, as shown in Fig. 5, was performed using the statistical analysis proposed by Stepp (1972). The magnitude ranges of M_w 3.0 – 4.0, 4.0 – 5.0, 5.0 – 6.0, 6.0 – 7.0, 7.0 – 8.0, and ≥ 8.0, correspond to 60, 70, 100, 120, 150 and 260 years, respectively.

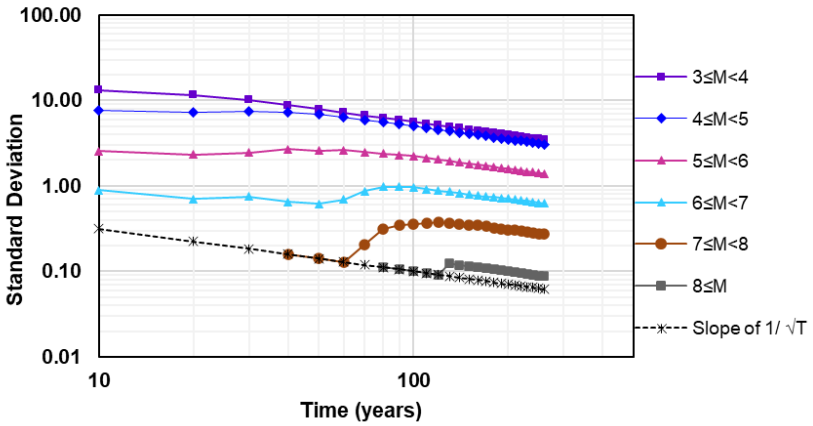

Fig. 5 Completeness of the earthquake catalogue with time

3.1.5 *Evaluation of Seismic Parameters*

The seismicity of a region can be described by seismic parameters *a* and *b*, which correlate with the rate of occurrence of an event of a particular size. The distribution of event sizes in a given period is best described by a most widely accepted Gutenberg-Richter recurrence law (Kramer 1996) as given by Eq. 1.

$$\log(N) = a - b(M_w) \tag{1}$$

Where *N* represents the number of cumulative events, per year, greater than an event of given moment magnitude; *a* and *b* are constants of regression, known as seismic parameters.

Based on the completeness study, the earthquake catalogue of the recent 70 years is considered to evaluate recurrence relation for each source zone (Fig. 6). The total number of earthquakes above the magnitude of completeness are 566, 431, 722, 2247, and 871 in the source zones 1, 2, 3, 4, and 5, respectively. The obtained values of seismic parameters *a* and *b* are summarized in Table 2.

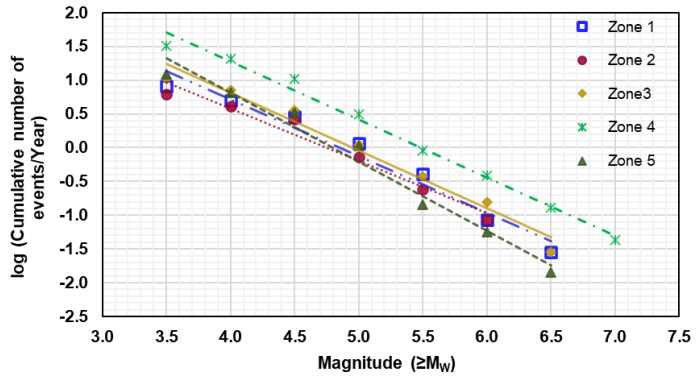

Fig. 6 Gutenberg-Richter relation for each source zone

Table 2 Seismic Parameters and M_C values

Source zones	M_C (using MAXC)	Seismic parameters		R^2
		a	*b*	

1	3.60	4.06±0.36	0.84±0.07	0.96
2	3.50	3.67±0.36	0.77±0.07	0.95
3	3.40	4.23±0.33	0.85±0.06	0.96
4	3.50	4.70±0.19	0.86±0.03	0.98
5	3.70	4.90±0.37	1.02±0.07	0.97

208

209 3.1.6 *Evaluation of Maximum Magnitude (M_{max})*

210 The largest possible earthquake, M_{max}, that a seismic source can produce ever is an important
211 input parameter for PSHA. In this study, M_{max} is evaluated based on the conventional
212 incremental value method, IVM (Gupta 2002; Anbazhagan et al. 2019) and the procedure
213 suggested by Kijiko and Sellevo (1989), typically referred to as *KS89*. A similar procedure has
214 been used by others as well (Sitharam and Sil 2014).

215 It is based on the doubly truncated G-R relation (Kijiko 2004) as given below.

216 $$M_{\max} = m_{\max}^{obs} + \Delta \text{ , where } \Delta = \frac{E_1(n_2) - E_1(n_1)}{\beta \exp(-n_2)} + m_{\min} \exp(-n) \qquad (2)$$

217 Where, M_{max} is the calculated maximum magnitude, $m_{\max}^{obs}$ is the observed maximum magnitude
218 associated with each fault, n is the number of events above M_C in the region and $m_{\min}$ denotes
219 the minimum magnitude. It should be mentioned here that the *KS89* procedure can be applied
220 only when the seismic parameter *'b'* of the region is known.

221 Based on M_C value, m_{min} in the present study is taken as 3.5 (M_w). $n_1 = \frac{n}{1 - \exp(-\beta(m_{\max} - m_{\min})}$

222 , $n_2 = n_1 \exp[-\beta(m_{\max} - m_{\min})]$, and $E_1(n_i)$ is an exponential integral function which can be

223 approximated as $E_1(n_i) = \frac{n_i^2 + a_1 n_i + a_2}{n_i(n_i^2 + b_1 n_i + b_2)} \exp(-n_i)$, where a_1 = 2.334733, a_2 = 0.250621, b_1

224 = 3.330657 and b_2 = 1.681534 (Abramowitz and Stegun 1970).

225 However, the incremental value method, which is relatively simple and applied by many
226 researchers, $M_{\max}$ is obtained by adding a constant value of 0.5 to $m_{\max}^{obs}$ value of each seismic
227 source (Gupta 2002; Anbazhagan et al. 2019; Bhuguna and Sil 2020). Values of M_{max}
228 calculated by both methods are given in Table 3.

229 3.1.7 *Deaggregation of Seismic Sources*

230 The recurrence relations for different seismic regions of the study area are evaluated, but it is
231 also essential to assess the seismic activity rate of each fault to proceed further with the PSHA.
232 For this purpose, an approach similar to Raghukanth and Iyenger (2006) and NDMA (2010) is
233 adopted in this study. A conservation property is heuristically used to develop recurrence
234 relations. The number of earthquakes per year with $M_w \geq m_{\min}$ i.e., $N(m_{\min} = 3.5)$ in a region
235 is calculated from the G-R relation of that region using Eq. 1. Since all these events are
236 associated with the faults within the region, it should be equal to the sum of the number of
237 earthquakes occurring on individual faults, i.e. $N(m_{\min}) = \sum_{i=1}^{n} N_i(m_{\min})$, where $N_i(m_{\min})$ is the
238 annual frequency of events of $M_w \geq m_{\min}$ on the i^{th} fault in the region, (i =1,2,3,…,n). The
239 annual frequency of events, $N_i(m_{\min})$ on any fault, depends on the fault length and past seismic
240 activity of the fault. The evaluation of $N_i(m_{\min})$ involves two basic assumptions: (1) longer
241 faults will have a higher capacity to rupture into smaller segments, and (2) shorter faults may
242 be more active in producing relatively smaller size events. Correspondingly, $N_i(m_{\min})$ is
243 obtained using the following equation

$$N_i(m_{\min}) = 0.5(\alpha_i + \chi_i) \cdot N(m_{\min}) \quad (3)$$

Where $\alpha_i = L_i / \sum L_i$ is the weighing factor for length of i^{th} fault (L_i), χ_i is another weighting factor defined as the ratio of the number of earthquakes associated with i^{th} fault to the total number of earthquakes in the region. In this study, 21 active seismic sources are identified and the detail of each fault in terms of the number of earthquakes associated with it, its length, weighing factors, and the evaluated maximum magnitude, are given in Table 3. The *b*-value of each fault is considered to be equal to the *b*-value of the region in which the fault is located, and the equation obtained is given below:

$$N_i(m) = N_i(m_{\min}) \left[1 - \frac{1 - e^{\{-\beta(m - m_{\min})\}}}{1 - e^{\{-\beta(m_{\max} - m_{\min})\}}} \right] \quad (4)$$

Where, $m_{\min}$ is the minimum threshold magnitude, $m_{\max}$ is the maximum potential magnitude of the fault *i,* and $\beta = 2.303b$. The individual fault level recurrence relations are shown in Figs. 7a-e.

3.1.8 *Ground Motion Prediction Equation (GMPE)*

The knowledge of site-specific attenuation relation is significant for the evaluation of GMP, but due to lack of good quality data, previously developed models for the same or of other regions based on similar tectonic features can be used (Nath and Thingbaijam 2012; Das et al. 2016).

In the present study, six GMPEs are selected (Table 4) and validated through the recorded strong motion data obtained from the NER of India. For this purpose, PGA vs hypocentral distance graphs, shown in Fig. 8a-e, are obtained for different combinations of magnitude and focal depth using the selected GMPEs given in Table 4. The observed PGA values from strong ground motion records for the same magnitude focal depth (M_w, h) combination are also

plotted, as shown in Fig. 8(a-e). It can be seen that irrespective of the M_w and h combinations, ANBA2013 and NATH2012 predicted PGA values are relatively lower than the observed ones. Besides, ATBO2003 is found to have overestimated the PGA for shorter distances and underestimated for longer distances (Fig.8). BAHU2020 also underestimates the PGA, making it the lower bound in few cases. For focal depths greater than 45 km, the PGA values given by the JAIN2000 model lies in the range of observed values, and for lesser depth, the RAMK2020 model is found to be more appropriate. Therefore, in the present study, GMPEs RAMK2020 (Ramkrishnan et al. 2020) is adopted for seismic source zones with an average focal depth of less than 45 km and JAIN2000 (Jain et al. 2000) is adopted for seismic source zones with an average focal depth greater than or equal to 45 km, respectively.

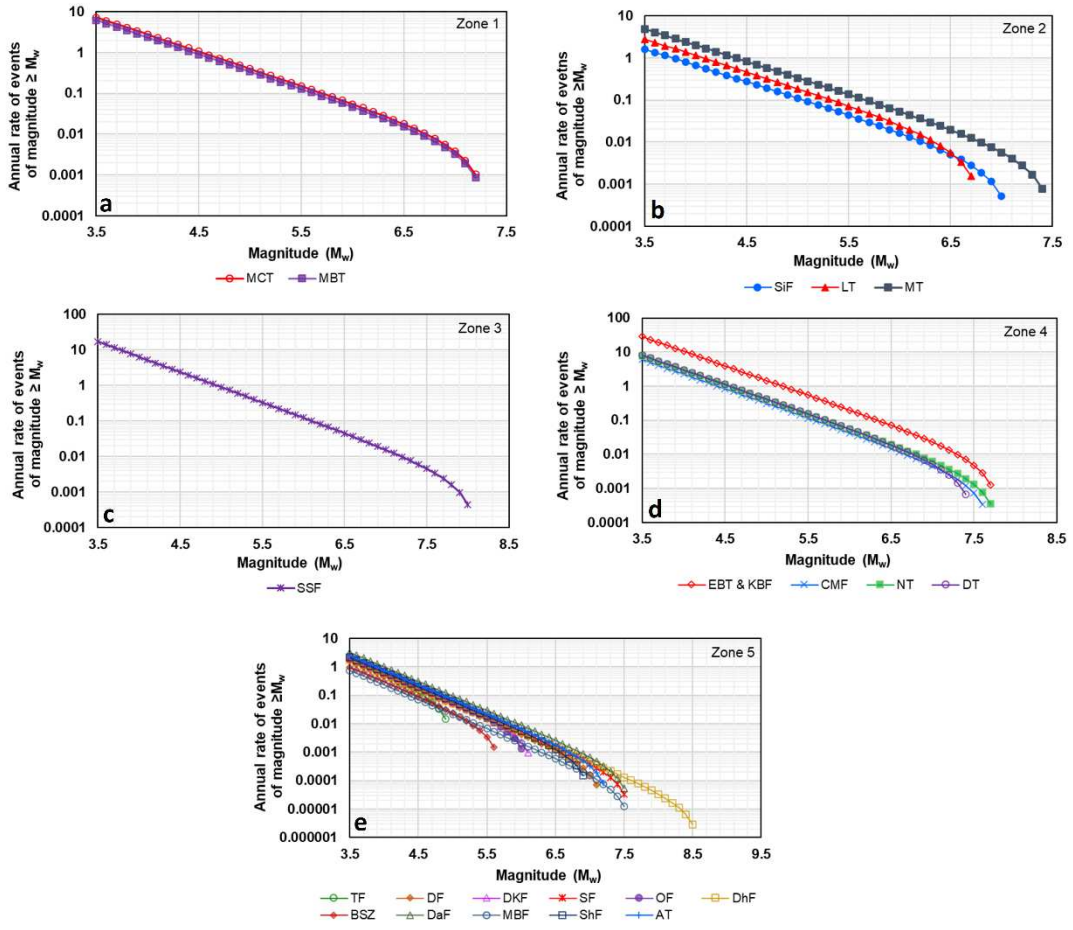

Fig. 7 Fault level recurrence relation for source (a) zone 1, (b) zone 2, (c) zone 3, (d) zone 4, and (e) zone 5

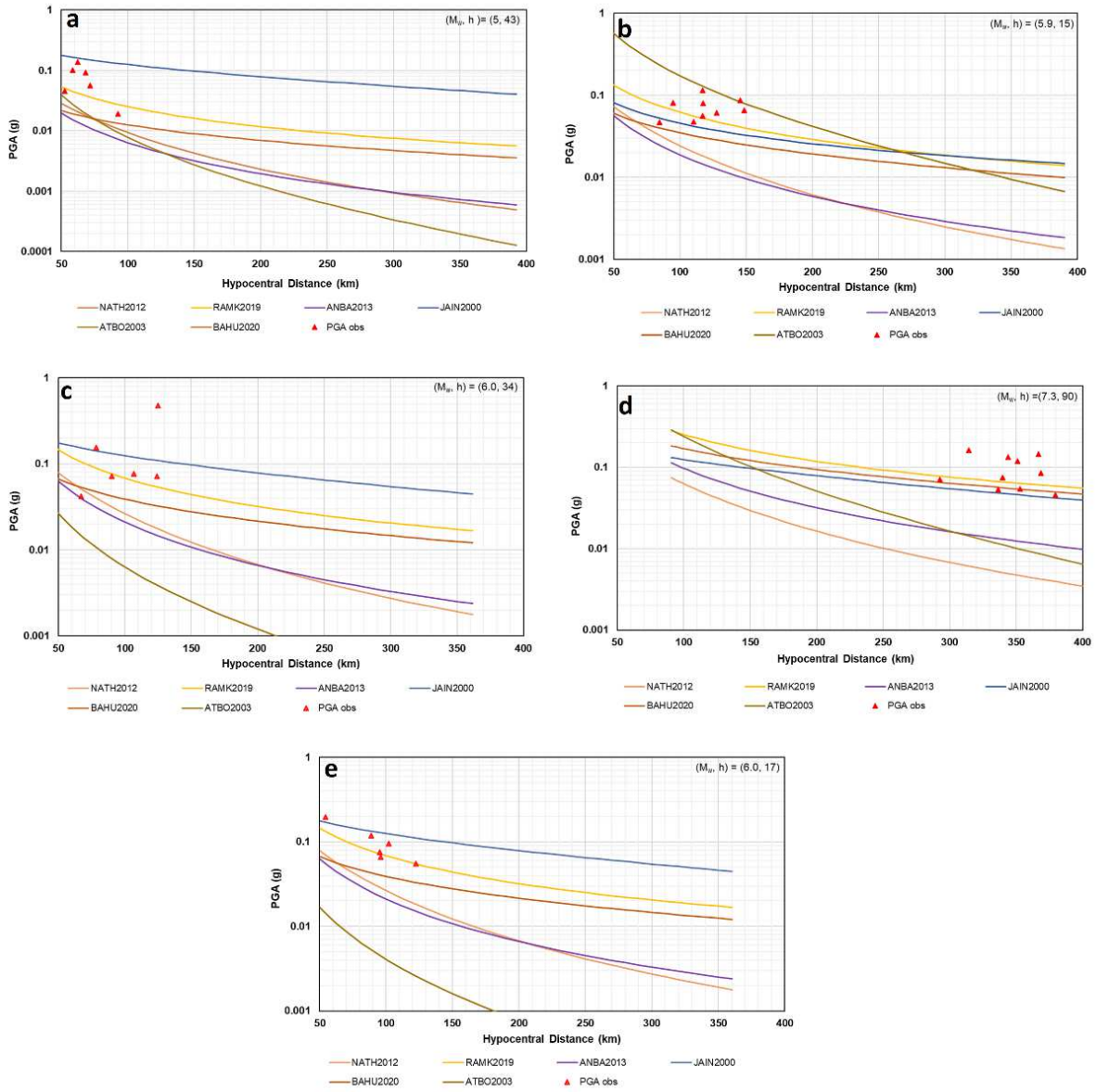

279

280 **Fig. 8** Comparison of GMPEs with the observed PGA values for a different combination of
281 moment magnitude and hypocentral distance (km): (a) M_w 5.0, h 43, (b) M_w 5.9, h 15, (c)
282 M_w 6.0, h 34, (d) M_w 7.3, h 90, (e) M_w 6.0, h 1

283

284 **Table 3** Seismic source zone characterization of the study area

Source zones	Fault name	Fault ID	Events associated with each fault	Length (km)	α_i	χ_i	Observed M_{max}	Calculated M_{max}	
								IVM	*KS89*
1	Main Central Thrust (MCT)	1	345	631.43	0.49	0.59	6.8	7.3	6.86
	Main boundary Thrust (MBT)	2	242	654.35	0.51	0.41	6.8	7.3	6.86
	Siang Fault (SiF)	3	73	87.47	0.18	0.16	6.6	7.1	6.63
2	Lohit Thrust (LT)	4	180	94.79	0.20	0.40	6.3	6.8	6.32
	Mishmi Thrust (MT)	5	194	293.11	0.62	0.43	7	7.5	7.06
3	Shan-Sagaing Fault (SSF)	6	750	704.60	1.00	1.00	7.6	8.1	7.96
	Eastern boundary thrust and Kabaw Fault (EBT & KBF)	7	1619	821.53	0.42	0.71	7.3	7.8	7.49
4	Chaurachandpur-Mao Fault (CMF)	8	345	174.39	0.09	0.15	7.2	7.7	7.35
	Naga Thrust (NT)	9	143	481.99	0.25	0.06	7.3	7.8	7.49
	Disang Thrust (DT)	10	180	475.78	0.24	0.08	7	7.5	7.10

5	Tista Fault (TF)	11	19	250.13	0.15	0.02	4.5	5	4.50
	Dhubri Fault (DF)	12	60	146.87	0.09	0.07	6.7	7.2	6.87
	Dhansiri-Kopili Fault (DKF)	13	104	135.95	0.08	0.11	5.7	6.2	5.72
	Samin Fault (SF)	14	120	84.86	0.05	0.13	7.1	7.6	7.64
	Oldham Fault (OF)	15	115	152.15	0.09	0.13	5.6	6.1	5.61
	Dhudhnoi Fault (DhF)	16	101	90.80	0.05	0.11	8.1	8.6	8.54
	Barapani Shear Zone (BSZ)	17	57	49.58	0.03	0.06	5.2	5.7	5.20
	Dauki Fault (DaF)	18	117	293.36	0.18	0.13	7.1	7.6	7.64
	Madhupur Blind Fault (MBF)	19	29	64.21	0.04	0.03	7.1	7.6	7.64
	Shylet Fault (ShF)	20	98	156.98	0.09	0.11	6.5	7	6.60
	Arakan Trench (AT)	21	86	222.04	0.13	0.09	6.8	7.3	7.01

285

286 **Table 4** List of selected GMPEs

Sl. No.	GMPE	Abbreviation	Remark
1	Jain *et al.* (2000) (a) non-subduction zone: $\ln(PGA) = -3.443 + 0.706M - 0.8028\ln(R)$ with SE = 0.44	JAIN2000	For Central-Himalayan region

	(b) subduction zone: $\ln(PGA) = -0.332 + 0.00233R + 0.59\ln(R)$ with SE = 0.59 Where PGA in g, R is the shortest source-to-site distance, and SE is the standard error		
2	Atkinson and Boore (2003) $\log Y = c_1 + c_2 M + c_3 h + c_4 R - g \cdot \log R + s_I (c_5 S_C + c_6 S_D + c_7 S_E)$ where Y in cm/s^2, $R = \sqrt{D_{fault}^2 + \Delta^2}$, $\Delta = 0.00724 \times 10^{(0.507M)}$, $c_1 = 2.991$, $c_2 = 0.03525$, $c_3 = 0.00759$, $c_4 = -0.00206$, $g = 10^{(1.2-0.18M)}$, $\sigma_1 = 0.20$(intra-event) and $\sigma_2 = 0.11$(inter-event) for interface events (h<50km) and $c_1 = -0.04713$, $c_2 = 0.6909$, $c_3 = 0.01130$, $c_4 = -0.00202$, $g = 10^{(0.301-0.01M)}$, $\sigma_1 = 0.23$ and $\sigma_2 = 0.14$ for in-slab events (h>50km) and $(c_5, c_6, c_7) = (0.19, 0.24, 0.29)$ for all events. s_I is frequency-dependent constant. S_C, S_D, and S_E are equal to zero for site class B (NEHRP), $V_{S,30}$ > 760m/s.	ATBO2003	
3	Nath *et al.* (2012) $\ln(P) = 9.143 + 0.247M - 0.014(10 - M)^3 - 2.67\ln(r_{rup} + 32.9458\,e^{(0.0663M)})$ where P = PGA (g), r_{rup}= fault-rupture distance (km). Standard Deviation = 0.330.	NATH200	For the Shillong region of NE India
4	Anbazhagan, Kumar and Sitharam (2013) $\log(y) = -1.283 + 0.544M + b \cdot \log(X + e^{(0.381M)}) + \sigma$ where Y = Spectral acceleration (SA) (g), $X = \sqrt{R^2 + h^2}$, where R = epicentral distance (km), h = focal depth (km), b is decay parameter (-1.792), and σ= 0.283 (for 0 s period).	ANBA2013	For Himalayan region
5	Ramkrishnan, Sreevalsa and Sitharam (2020)	RAMK2020	

	$\log y = -2.135 + 0.437M - 1.099\log(X + e^{(-0.080M)}) \pm 0.549$ where y = PGA (g), X = hypocentral distance (km), and SE = ±0.549		For Central-Himalayan region
6	Bahuguna and Sil (2020) $\ln(PGA) = 6.680 + 1.134M - 0.001R - 0.7098\ln R$ where PGA in g, R = hypocentral distance (km) (ranges from 100-400km), and standard deviation = 0.53	BAHU2020	For Assam region

Where, M is moment magnitude

3.1.9 *PSHA of NER India*

In order to evaluate seismic hazard at bedrock level, using a probabilistic approach, the entire study area was divided into a grid size of 0.2° x 0.2°. Each grid centre is considered as the site of interest at which the seismic hazard in terms of PGA is evaluated by considering all the active seismic sources within a radius of 500 km.

The procedure followed for PSHA assumes that an event within a seismic source follows a stationary Poisson process (Kramer 1996). The probability of GMP, *Y*, exceeding a specified level, *y*, in a specified period *T*, at a given site is expressed as

$$P(Y > y) = 1 - \exp(\mu_y T) \tag{6}$$

Where, μ_y is the mean annual rate of exceedance as detailed below

$$\mu_y = \sum_{i=1}^{n} N_i(m_{\min}) \int_m \int_r P(Y > y \mid m, r)\, p_{R|M}(r \mid m)\, p_M(m)\, dr\, dm \tag{7}$$

In this equation, *n* is the total number of faults present, $N_i(m_{\min})$ is the annual frequency of events on an i^{th} fault having $m \geq m_{\min}$, $p_M(m)$ is the probability density function (PDF) corresponding to the magnitude, $p_{R|M}(r \mid m)$ is the conditional PDF corresponding to hypocentral distance (*r*), and $P(Y > y \mid m, r)$ is the probability of exceedance of GMP, *Y*, over *y*, for an event of magnitude *m* occurring at a distance *r* from the site. μ_y incorporates the temporal, spatial, and magnitude uncertainty of a future event and ground motion uncertainty produced by them at the site. Eq. 7 shows the summation of individual contributions of 21 faults ($i = 1, 2, 3 \ldots 21$) for the assessment of hazard at each site to obtain the annual exceedance of PGA. All the above-mentioned calculations are performed using MATLAB.

The typical PDF of magnitude and distance is shown in Fig. 9. To produce the hazard curve considering all the sources, μ_y of a particular site of interest are summed up and plotted against

the target PGA level, y. Fig. 10 shows the hazard curves for Shillong city. Using the hazard curves, the PGA value for 10% probability of exceedance over 50 and 100 years of return period and 2% probability of exceedance over 50 years of return period are obtained. Correspondingly, thematic maps, at each site of interest, are produced using ArcGIS.

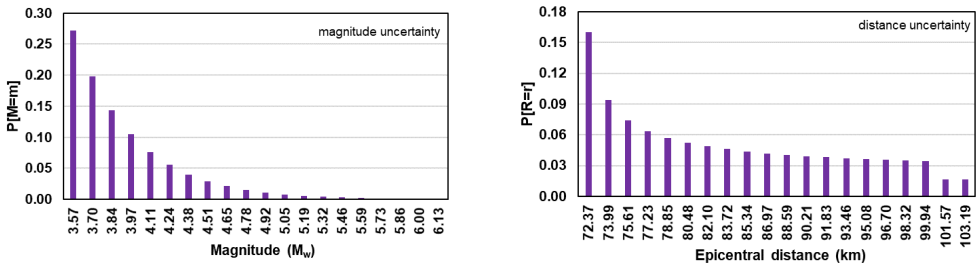

Fig. 9 Probability density function (PDF) for (a) magnitude uncertainty, (b) epicentral distance uncertainty

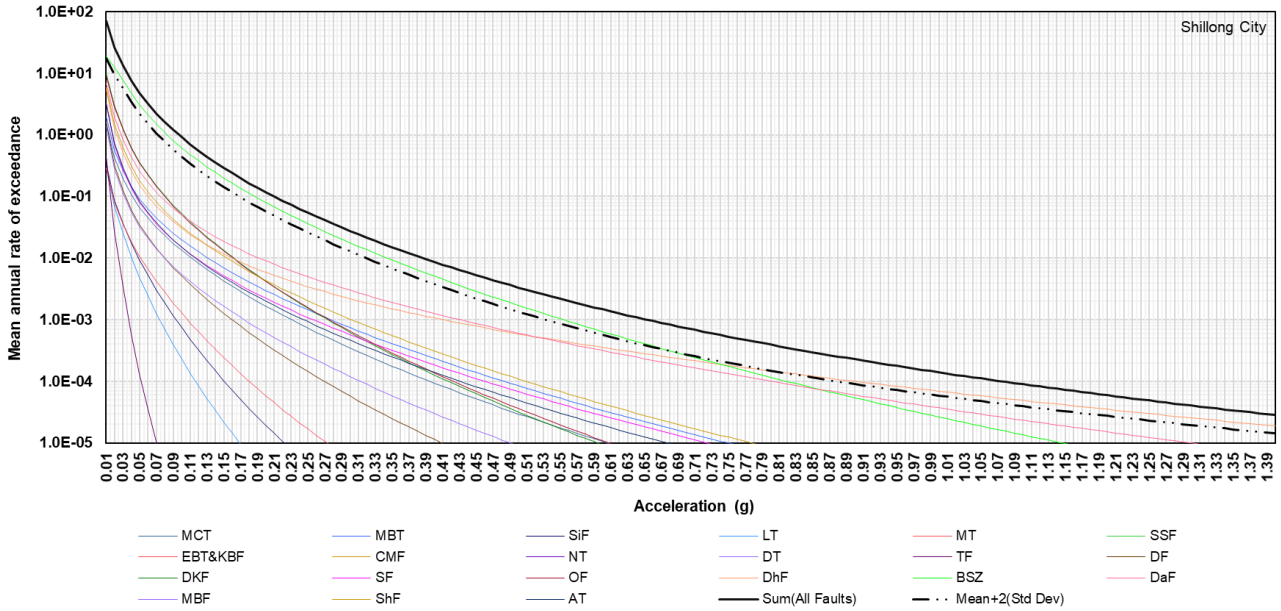

Fig. 10 Seismic hazard curves (Shillong city)

3.2 *Social Vulnerability Assessment*

In the present study, the HoP model is adopted for assessing the social vulnerability (SV) of different districts of SSS. The HoP model (Cutter 1996) tries to combine social and biophysical vulnerability to produce overall place vulnerability (Cutter et al. 2003). This model has been used in many social vulnerability studies worldwide (Ge et al. 2013; Frigerio et al. 2016;

Agrawal et al. 2021). Details of the methodology adopted for the social vulnerability analysis, SVA are presented and discussed in the following subsections.

3.2.1 *Data Acquisition*

The social vulnerability assessment depends on the indicators like population, age, gender, literacy, employment status, stock of built structures, etc. (Cutter et al. 2003; Wood et al. 2010; Depietri 2013, 2020; Kolathayar 2021; Siagian et al. 2014; Fatemi et al. 2017). For the present study, data regarding these indicators comprising 54 variables were collected, at the district level, from India's 15th housing and population census (Census 2011). Multi-collinearity analysis was performed on the collected set of variables, and a subset of 33 variables was retained and used to create indices for SV in Table 5.

Table 5 List of common social vulnerability indicators and their variables.

Sl. No.	Indicator		Variables
1	Population composition	P01	Population density
2		P02	Male (%)
3		P03	Female (%)
4		P04	Population belongs to socially backward class (%)
6	Age	Age01	Age less than 07 (%)
7		Age02	Age group of 07 to 60 (%)
8		Age03	Above the age of 60 (%)
9	Literacy	L01	Effective literacy rate
10		L02	Illiterate (%)
11		L03	Illiterate female (%)
12	Employment status and occupation	EO01	Population belongs to MW[1] class (%)
13		EO02	Female population belongs to MW[1] class (%)
14		EO03	Population belongs to the OMW[2] class (%)
15		EO04	Female population belongs to the OMW[2] class (%)
16		EO05	Population belongs to MrW[3] class (%)
17		EO06	Female population belongs to MrW[3] class (%)
18		EO07	Population belongs to the OMrW[4] class (%)
19		EO08	Female population belongs to the OMrW[4] class (%)
20		EO09	Non-permanent employment (%)
21		EO10	Female population with non-permanent employment (%)
22		EO11	Non-working population (%)
23		EO12	Non-working female population (%)
24	Building material	BM01	With brick or stone roof (%)
25		BM02	With kutcha roof (%)

26		BM03	With kutcha wall (%)
27		BM04	With kutcha floor (%)
28	House condition	HC01	Residential houses in dilapidated condition (%)
29		HC02	Residential cum other houses in dilapidated condition (%)
30	Family size	HH01	Houses with 4-5 households (%)
31		HH02	Houses with 6 or more households (%)
32	Amenities	A01	Houses with no electricity and have dependence upon kerosene or other oil as a source of light (%)
33		A02	Houses with no water source within or near the premises of the house (%)

[1]MW: Main Workers; Workers who worked for more than six months in the reference period

OW: Other Workers; Workers other than cultivators, agricultural laborers, or household workers. eg. Government servants, municipal employees, teachers, bankers, trade and commerce, etc.

[2]OMW: Other Main Workers; Main workers falling under OW

[3]MrW: Marginal Workers; Workers who worked for less than six months

[4]OMrW: Other Marginal Workers; Marginal worker falling under OW

3.2.2 *Evaluation of SVI*

The social vulnerability index (SVI) is evaluated using the steps summarized below.

1. Variables of vulnerability indicators are selected, and high multi-collinearity among the variables is checked.
2. After eliminating the highly correlated variables, the remaining set of variables are checked for sample adequacy using KMO (Kaiser-Meyer-Olkin) and Bartlett's test. If the KMO value > 0.7 and Bartlett's test of sphericity shows a significance value < 0.05, the dataset is considered adequate, and the factor analysis (FA) is employed (Sharma 1996).
3. The principal component analysis (PCA) is utilized for factor extraction. Factors with eigenvalue > 1.0 are extracted and rotated using the varimax method of factor rotation with Kaiser normalization, as shown in Table 6. The extracted factors are confirmed by tracking the changes in the slop of the scree plot shown in Fig. 11.
4. The factor score is generated for extracted factors using the Anderson-Rubin method. All these steps are performed using IBM SPSS (v 26).

5. The generated scores are aggregated (Ge et al. 2013), and a composite index (SVI) is generated using the weightage factor (w_i), calculated based on the percentage variance explained by factor i (v_i) out of the total variance explained by all the factors (v_t) as in Eq. 8. Then the composite SVI is obtained by using Eq. 9.

$$w_i = v_i / v_t \tag{8}$$

$$SVI = \sum_{i=1}^{n_f} w_i \times \text{Factor i} \quad \text{, where } n_f \text{ is the number of factors} \tag{9}$$

6. The SVI scores are classified into five vulnerability classes, and thematic maps are created to display the spatial distribution of social vulnerability using ArcGIS.

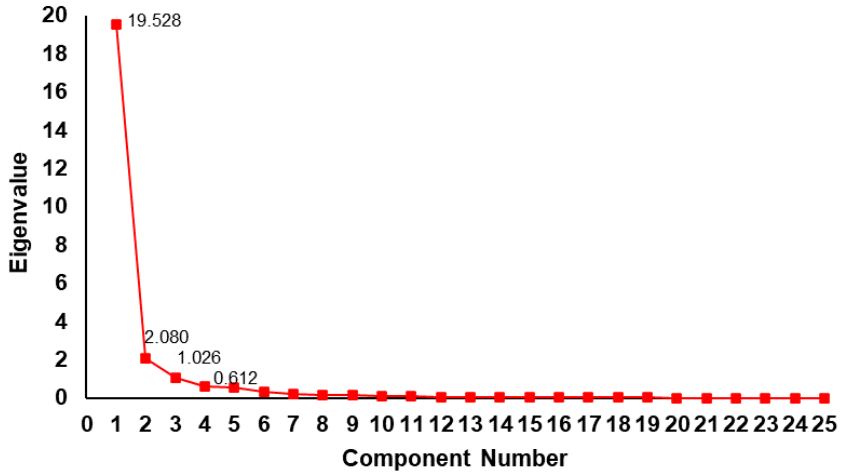

Fig. 11 Scree plot

Table 6 Selected variables based on PCA

Factor	Extracted variables	Eigenvalue	Variance explained (%)	Weightage factor (w_i)
1	HC01, A01, L02, P02, L03, Age01, HC02, BM03, EO12, HH02, EO11, BM02, and A02	19.528	37.87	0.42
2	BM01, EO03, EO07, HH01, Age03, and P04	2.080	27.35	0.30

3	EO02, EO06, EO05, EO10, and EO01	1.026	25.31	0.28

3.2.3 *Spatial Cluster Analysis*

A global spatial autocorrelation is performed to analyze the autocorrelation of the dataset throughout the study area, and Global Moran's I value that ranges from -1 to 1, was obtained (Karuppusamy et al. 2021). A spatial statistical tool for hotspot analysis (Getis-Ord Gi*) in ArcGIS is employed to identify the spatial clusters within a specific area (Brandt et al. 2020). The hotspots are located based on the values of statistically significant *z* for 99, 95, and 90 % confidence levels. Typically the hotspots exhibit higher *z* scores and lower *p* scores (Al-Dogom et al. 2018). In this analysis, a zone of indifference is selected for the spatial relationship conceptualization, and a threshold distance of 71542 m is used. False discovery rate (FDR) correction is applied to identify spatial clusters at the local level better.

3.3 *Exposure Assessment*

For the seismic exposure assessment, the PGA values for the 475-year return period are classified into five hazard classes (Fig. 17a) and integrated with the SVI. The resulting seismic exposure map (Fig. 17b) was analyzed using a risk matrix) (Derakhshan et al. 2020) as shown in Fig 12.

		Hazard Classes				
		Very Low (1)	Low (2)	Moderate (3)	High (4)	Very High (5)
Social Vulnerability	Very low (1)	1	2	3	4	5
	Low(2)	2	4	6	8	10
	Moderate(3)	3	6	9	12	15
	High(4)	4	8	12	16	20
	Very High (5)	5	10	15	20	25
Risk Classes		Very Low	Low	Moderate	High	Very High

Fig. 12 Risk matrix

4. Results and Discussion

In the present study, the results of PSHA are presented in terms of PGA at bedrock level, which is obtained from the hazard curve i.e. PGA vs. mean annual rate of exceedance. The SVI was generated by applying the FA and PCA as the factor extraction method. The results of SHA and SVI were then integrated to prepare the exposure maps for the study region.

From Table 7, it can be seen that the seismic parameters, *a* and *b*, obtained from the present study, compare well with the values reported by others (NDMA 2010; Sharma and Malik 2006; and Bahuguna and Sil 2020). For SSS in the present study, the PGA values corresponding to return periods of 475, 950, and 2475 years, obtained using GMPE (Ramkrishnan et al. 2020, Jain et al. 2000), are in the range of 0.14-0.69g, 0.17-0.86g, and 0.22-0.93g, respectively. The calculated PGA values for some selected cities in the region are compared with those from previous studies as shown in Table 8. It can be seen that the calculated PGA values in the present study are relatively lower than those reported by Nath and Thingbaijam (2012). In the case of cities like Aizwal, Imphal, and Kohima, the PGA values for low probability of exceedance (return period = 475 years) are comparable with that of NDMA 2010 (Table 8). In contrast, at Aizwal and Imphal, the calculated PGA values are less than that reported by Sharma and Malik (2006) and higher than that by Sil et al. (2013). At Guwahati and Shillong, the calculated PGA values are in a higher range than that reported by Ghione et al. (2021). Such variations are attributed to the selection of different seismic source zones and different ground attenuation models, which can be considered as a limitation of the PSHA method.

The spatial distributions of PGA at the bedrock level for SSS are shown in Fig. 13a-c. The northern and western part of the region shows higher PGA values. This is due to the influence of MFT, MCT, and Dauki Fault. Similarly, the area in the vicinity of Mishimi Thrust and Lohit

Thrust also shows higher PGA values. Therefore, this region can be classified as a high seismic hazard zone.

Table 7 Comparison of estimated seismic parameters with previously reported values

Parameter	Das, Sharma, and Wason (2016)	NDMA (2010)	Sharma and Malik (2006)	Bahuguna and Sil (2020)	Present study
a	1.68-5.76	-	-	0.15-4.52	3.67-4.89
b	0.43-1.07	Zone4: 0.71±0.04 Zone5: 0.66±0.03 Zone7: 0.67±0.08 Zone8: 0.73±0.04 Zone10: 0.80±0.02 Zone11: 0.66±0.04	0.42-1.04	0.18-0.9	0.77-1.02
M_c	3.6-4.6	-	-	-	3.4-3.7

Table 8 Comparison of estimated PGA values obtained for important cities with previously reported values

Sl. No.	City	PGA (g)			
		Present Study‡	NDMA (2010)†	Nath and Thingbaijam (2012)‡	Other studies
1	Guwahati	0.60-0.85	0.23-0.40	0.66-1.40	0.35 (Ghione, Poggi and Lindholm 2021)*; 0.46-0.92 (Bahuguna and Sil 2020)†,
2	Agartala	0.32-0.47	0.12-0.20	0.25-0.60	0.22 (Das, Sharma and Wason 2016)*; 0.11-0.20 (Sil, Sitharam and Kolathayar 2013)‡
3	Aizawl	0.20-0.32	0.22-0.45	0.45-1.20	0.3 (Sharma and Malik 2006)*; 0.1-0.17 (Sil, Sitharam and Kolathayar 2013)‡
4	Imphal	0.28-0.42	0.30-0.55	0.70-1.40	0.4(Sharma and Malik 2006)*; 0.18-0.8 (Pallav *et al.* 2012)‡
5	Shillong	0.61-0.83	0.25-0.45	0.72-1.30	0.55 (Ghione, Poggi and Lindholm 2021)*

6	Itanagar	0.55-0.88	0.28-0.45	0.70-1.20	0.44(Sharma and Malik 2006)*; 0.18 (Das, Sharma and Wason 2016)*
7	Kohima	0.25-0.40	0.25-0.55	0.60-1.30	0.5 (Sharma and Malik)*; 0.15(Das, Sharma and Wason 2016)*

For return period of * 475 years; ‡ 475–2475 years; † 475–4950 years

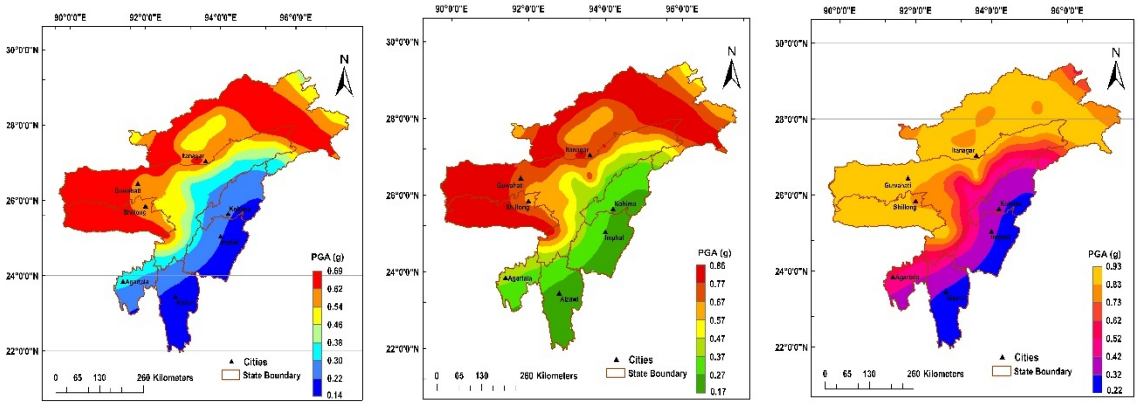

(a) (b) (c)

Fig. 13 Spatial distribution of PGA at the bedrock level for a return period of (a) 475 years, (b) 950 years, and (c) 2475 years

The SVI for the study area is developed considering three significant factors that are obtained by FA. Based on PCA of 33 variables, using Kaiser criterion of factor retention, three significant factors comprised of 24 variables with eigenvalues >1.0 are retained. The KMO value of 0.897 (>0.7) and a significant value of 0 (<0.05) in Bartlett's test are obtained that indicates sufficient data adequacy for statistical analysis (FA and PCA). The selection of factors is also confirmed by observing the change in slope of the scree plot (Fig. 11). These three factors cumulatively explain the 90.534 percent variance among the datasets. The descriptive statistic of each factor is given in Table 6.

The variable composition of factor 1 indicates the living condition and socioeconomic status of the study region. The spatial distribution of vulnerability in terms of factor 1 is shown in Fig. 14a. The districts of Assam and Tripura, having a high percentage of illiterate population, with poor living conditions, fall under the high to very high vulnerable class. Hence, it can be

said that communities with high illiteracy rates and poor living conditions are less resilient and thereby more vulnerable to seismic disasters. Similar observations have been made by (Frigerio et al. 2016). Factor 2 comprises six variables, governed by building material, aged population, and period of employment. Based on these indices it is observed that the region of Tripura, upper Assam, and Barak valley have a poor quality of built structures, low employment rate, and a high population of old aged people (Fig 14b). All these factors tend to enhance the vulnerability of a region and decrease the society's resilience and coping capacity in case of a disastrous event happening. Factor 3 represents the type of employment and percentage of the female population involved in agriculture and other related activities (Fig. 14c). The Seven Sister States of India with a primary focus on agriculture is relatively less urbanized. Agriculture and small-scale household industries are low-paying jobs, and the female population of this region is found to be mainly involved in it. After the disaster, the non-permanent marginal workers having relatively low-paying jobs, are more likely to lose their jobs due to disruption in daily activities and businesses (Morrow 1999). The spatial distribution of Factor 3 shows that the districts of Assam, Meghalaya, Mizoram, and Manipur, having a high percentage of the population dependent on agriculture and small-scale industries, are under a highly vulnerable class.

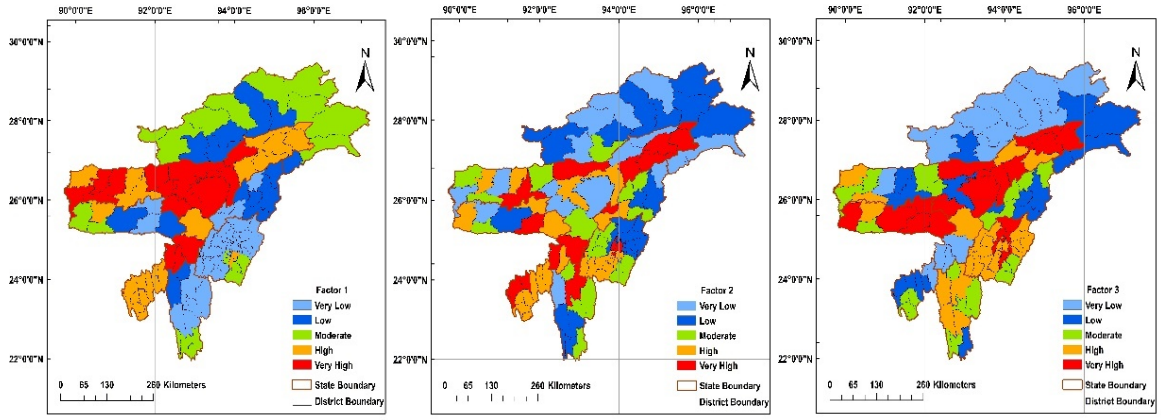

(a) (b) (c)

Fig. 14 Spatial distribution of social factors (a) Factor 1, (b) Factor 2, and (c) Factor 3

Fig. 15 shows the spatial distribution of the overall social vulnerability at the district level. It reveals that most districts covering an area of 66.15% of the study area are under low to moderate SVI class, whereas another 14.56% area is under high vulnerability and 19.29% of the area is prone to very high vulnerability. Twenty-one districts of Assam fall under high and very high vulnerable classes, and all districts of Tripura are under high vulnerable classes. These two states share the highest percentage of the population in the study region (i.e., 69.41% for Assam and 8.01% for Tripura). With a population density of 439.43 per sq. km in Assam and 389.11 per sq. km in Tripura and according to the 2011 census data (Fig. 1), 40% population of these districts are illiterate, and about 83% of houses are made of weak building materials are of poor quality. These districts also lack basic amenities like the availability of drinking water, electricity, etc. These factors justify the very high social vulnerability of these districts.

The spatial cluster analysis given in Fig. 16a represents hotspot and cold spot analysis. Fig. 16b depicts an overlay of the spatial distribution of the social vulnerability index with hotspots and cold spots. It is observed that high social vulnerability patterns are located in central Assam and its adjoining neighboring areas, and 17.14% of the total study area emerges as a hot spot with an average SVI score of 0.329. The cold spots are mainly predominant in Nagaland and the northern part of Arunachal Pradesh, spread over about 8.58% of the study area, with an average SVI score of 0.177. With an average SVI score of 0.208, the remaining area is regarded as non-significant areas in terms of the hotspot and cold spot analysis, and those are the north-western and southern parts of the study area.

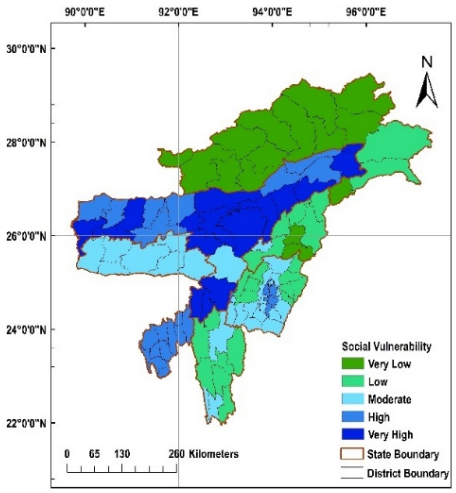

Fig. 15 Spatial distribution of social vulnerability index

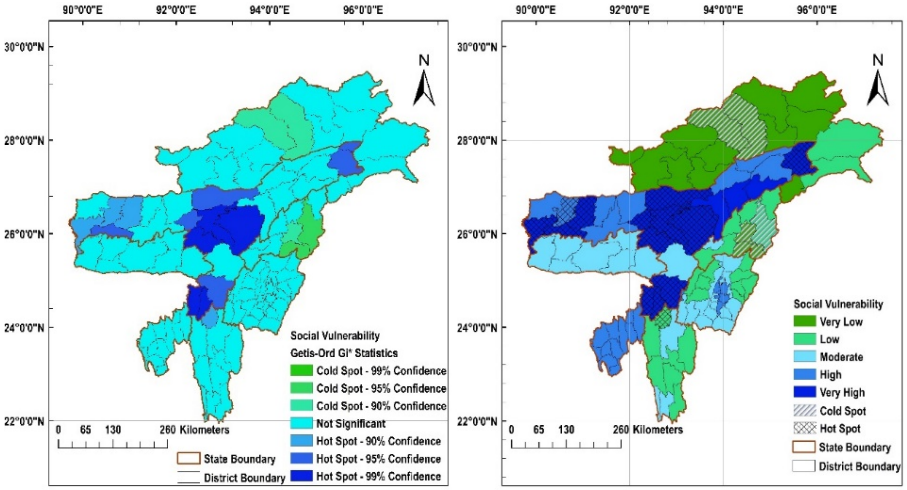

Fig. 16 (a) cluster showing hotspot and cold spot; (b) overlay of a hotspot and cold spot with SVI

Finally, the seismic hazard map (Fig 17a) is integrated with the social vulnerability map (Fig 15), and the exposure map of the study area is prepared and analyzed using the risk matrix in Fig. 12. Fig. 17b shows the spatial distribution of exposure to seismic hazards for the NER of India. The results indicate that 3.33%, 38.21%, 29.94%, 14.59%, and 13.92% of the total study area falls under very low, low, moderate, high, and very high seismic exposure classes, respectively. The districts of Arunachal Pradesh, Nagaland, and Mizoram mostly fall under very low to moderate seismic exposure classes. Low to moderate seismic exposure zones are found for the districts of Manipur and Tripura. In contrast, the districts of Assam and Meghalaya shows high to very high seismic exposure class.

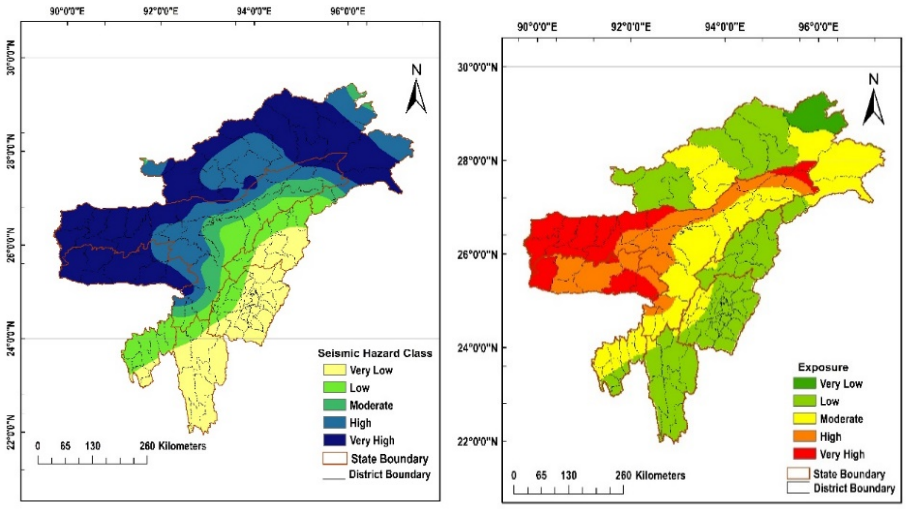

(a) (b)

Fig. 17 (a) seismic hazard class; (b) exposure

5. Conclusions

In the present study, updated seismic hazard maps in terms of PGA for the return periods of 475, 950, and 2475 years are generated using the PSHA approach. Correspondingly the PGA values at bedrock level are found to be in the range of 0.14-0.69g, 0.17-0.86g, and 0.22-0.93g, respectively. The states of Meghalaya, Assam, and Arunachal Pradesh exhibit relatively higher PGA values, which is attributed to the dominance of the MFT, Dauki fault, and Mishimi thrust zone. The SVI map is generated using FA and PCA to assess the social vulnerability and exposure to seismic hazards. Based on PCA, three factors consisting of 24 variables are retained, which explains the 90. 53% variance among the datasets. Subsequently, the SVI is integrated with the seismic hazard map and an exposure map of the study area is developed.

The spatial distribution of SVI shows that 21 districts covering 91.43% area of Assam and the entire Tripura state are highly vulnerable. The spatial cluster analysis illustrates high social vulnerability patterns in central Assam and some parts of Meghalaya, Mizoram, Manipur, and Arunachal Pradesh. 17.14% of the study area, having an average SVI score of 0.329, is identified as hotspots. The exposure map shows that more than 50% of the total study area falls under moderate to very high exposure class. The present study provides a reliable tool for

identifying the most socially vulnerable and critically exposed areas of one of the most seismically active regions of the world, i.e. NER of India. The findings from the present study can be of help in sustainable disaster mitigation planning leading to achieving sustainable development goals and targets. The presented exposure map can help the state authorities and local bodies in preparing for disaster risk reduction, develop mitigation strategies, and emergency planning. The study has some inherent limitations which are due to the lack of real-time socio-economic data. Therefore further research considering geotechnical, geological data, and temporal relationships among the various socioeconomic variables and various hazards, is necessary.

Declaration of interests

The authors declare that they have no known competing financial interests or non-financial interests or personal relationships that are directly or indirectly related to the work submitted for publication that could have appeared to influence the work reported in this paper.

CRediT authorship contribution statement

Conceptualization: Jagabandhu Dixit; Methodology: Navdeep Agrawal, Laxmi Gupta, Jagabandhu Dixit; Formal analysis and investigation: Navdeep Agrawal, Laxmi Gupta; Validation: Navdeep Agrawal, Laxmi Gupta, Jagabandhu Dixit; Visualization: Navdeep Agrawal, Laxmi Gupta; Writing - original draft preparation: Navdeep Agrawal, Laxmi Gupta; Writing - review and editing: Jagabandhu Dixit, Sujit Kumar Dash; Resources: Jagabandhu Dixit; Supervision: Jagabandhu Dixit

References

Abramowitz M, Stegun IA (1972) Handbook of mathematical functions: with formulas, graphs, and mathematical tables. National Bureau of Standards Washington, DC:(Vol 55, 319)

529 Agrawal N, Gupta L, Dixit J (2021) Assessment of the socioeconomic vulnerability to seismic
530 hazards in the National Capital Region of India using factor analysis. Sustainability
531 13(17):9652
532 Al-Dogom D, Schuckma K, Al-Ruzouq R (2018) Geostatistical seismic analysis and hazard
533 assessment, United Arab Emirates. International Archives of the Photogrammetry, Remote
534 Sensing and Spatial Information Sciences 42 (3/W4)
535 Anbazhagan P, Bajaj K, Matharu K, Moustafa SS, Al-Arifi NS (2019) Probabilistic seismic
536 hazard analysis using the logic tree approach–Patna district (India). Natural Hazards and
537 Earth System Sciences 19(10):2097-2115
538 Anbazhagan P, Kumar A, Sitharam TG (2013) Ground motion prediction equation considering
539 combined dataset of recorded and simulated ground motions. Soil Dynamics and
540 Earthquake Engineering 53:92-108
541 Armaș I, Gavriș A (2013) Social vulnerability assessment using spatial multi-criteria analysis
542 (SEVI model) and the Social Vulnerability Index (SoVI model)–a case study for Bucharest,
543 Romania. Natural Hazards and Earth System Sciences *13*(6):1481-1499
544 Atkinson GM, Boore DM (2003) Empirical ground-motion relations for subduction-zone
545 earthquakes and their application to Cascadia and other regions. Bulletin of the
546 Seismological Society of America 93(4):1703-1729
547 Bahuguna A, Sil A (2020) Comprehensive seismicity, seismic sources and seismic hazard
548 assessment of Assam, North East India. Journal of Earthquake Engineering 24(2):254-297
549 Baro O, Kumar A, Ismail-Zadeh A (2018) Seismic hazard assessment of the Shillong Plateau,
550 India. Geomatics, Natural Hazards and Risk 9(1):841-861
551 Bhukosh-Geological Survey of India (https://bhukosh.gsi.gov.in/Bhukosh/MapViewer.aspx),
552 (last assessed: 20 September 2021)

553 Brandt K, Graham L, Hawthorne T, Jeanty J, Burkholder B, Munisteri C, Visaggi C (2020)
554 Integrating sketch mapping and hot spot analysis to enhance capacity for community-level
555 flood and disaster risk management. The Geographical Journal 186(2):198-212
556 Birkmann J (2013) Measuring vulnerability to natural hazards: towards disaster resilient
557 societies. (i9789280811353). United Nations University Press, Tokyo, Japan
558 Census of India (2011) Provisional Population Totals. New Delhi: Office of the Registrar
559 General and Census Commissioner. https://censusindia.gov.in/
560 Cutter SL (1996) Vulnerability to environmental hazards. Progress in Human Geography
561 20(4): 529-539
562 Cutter SL, Barnes L, Berry M, Burton C, Evans E, Tate E, Webb J (2008) A place-based model
563 for understanding community resilience to natural disasters. Global Environmental Change
564 18(4):598-606
565 Cutter SL, Boruff BJ, Shirley WL (2003) Social vulnerability to environmental hazards. Social
566 Science Quarterly 84(2):242-261
567 Das R, Sharma, ML, Wason HR (2016) Probabilistic seismic hazard assessment for northeast
568 India region. Pure and Applied Geophysics 173(8):2653-2670
569 Das S, Hazra S, Haque A, Rahman M, Nicholls RJ, Ghosh A, Ghosh T, Salehin M, de Campos
570 RS (2021) Social vulnerability to environmental hazards in the Ganges-Brahmaputra-
571 Meghna delta, India and Bangladesh. *International Journal of Disaster Risk*
572 *Reduction* 53:101983.
573 Depietri Y, Welle T, Renaud FG (2013) Social vulnerability assessment of the Cologne urban
574 area (Germany) to heat waves: links to ecosystem services. International Journal of
575 Disaster Risk Reduction 6:98-117
576 Depietri Y (2020) The social–ecological dimension of vulnerability and risk to natural hazards.
577 Sustainability Science 15:587–604

578 Derakhshan S, Hodgson ME, Cutter SL (2020) Vulnerability of populations exposed to seismic
579 risk in the state of Oklahoma. Applied Geography 124:102295
580 Dixit J, Raghukanth STG, Dash SK (2016) Spatial distribution of seismic site coefficients for
581 Guwahati city. In *Geostatistical and Geospatial Approaches for the Characterization of*
582 *Natural Resources in the Environment* 533-537
583 Dutta SC, Halder L, Sharma RP (2021) Seismic vulnerability assessment of low to mid-rise
584 RC buildings addressing prevailing design and construction practices in the Northeastern
585 region of the Indian subcontinent: A case study based approach. Structures 33:1561-1577
586 Fatemi F, Ardalan A, Aguirre B, Mansouri N, Mohammadfam I (2017) Social vulnerability
587 indicators in disasters: findings from a systematic review. International Journal of Disaster
588 Risk Reduction 22:219-227
589 Frigerio I, Ventura S, Strigaro D, Mattavelli M, De Amicis M, Mugnano S, Boffi M (2016) A
590 GIS-based approach to identify the spatial variability of social vulnerability to seismic
591 hazard in Italy. Applied Geography 74:12-22
592 Gardner JK, Knopoff L (1974) Is the sequence of earthquakes in Southern California, with
593 aftershocks removed, Poissonian?. Bulletin of the Seismological Society of America
594 64(5):1363-1367
595 Ge Y, Dou W, Gu Z, Qian X, Wang J, Xu W, Shi P, Ming X, Zhou X Chen Y (2013)
596 Assessment of social vulnerability to natural hazards in the Yangtze River Delta, China.
597 Stochastic Environmental Research and Risk Assessment 27(8):1899-1908
598 Ghione F, Poggi V, Lindholm C (2021) A hybrid probabilistic seismic hazard model for
599 Northeast India and Bhutan combining distributed seismicity and finite faults. Physics and
600 Chemistry of the Earth, Parts A/B/C, 103029
601 Gupta ID (2002) The state of the art in seismic hazard analysis. ISET Journal of Earthquake
602 Technology 39(4):311-346

603 Indian Standard (2016) Criteria for earthquake resistance design of structures, Fifth revision,
604 Part-I, New Delhi
605 ISC, International Seismological Centre, ISC-GEM Earthquake Catalogue 2021, URL:
606 https://doi.org/10.31905/d808b825 (last accessed: 20 September 2021)
607 Jain SK, Roshan AD, Arlekar JN, Basu PC (2000) Empirical attenuation relationships for the
608 Himalayan earthquakes based on Indian strong motion data. In Proceedings of The Sixth
609 International Conference on Seismic Zonation 12-15
610 Karuppusamy B, Leo George S, Anusuya K, Venkatesh R, Thilagaraj P, Gnanappazham L,
611 Kumaraswamy K, Balasundareshwaran AH, Balabaskaran NP (2021) Revealing the socio-
612 economic vulnerability and multi-hazard risks at micro-administrative units in the coastal
613 plains of Tamil Nadu, India. Geomatics, Natural Hazards and Risk 12(1):605-630
614 Kijko A, Sellevoll MA (1989) Estimation of earthquake hazard parameters from incomplete
615 data files. Part I. Utilization of extreme and complete catalogues with different threshold
616 magnitudes. Bulletin of the Seismological Society of America 79(3):645-654
617 Kijko A (2004) Estimation of the maximum earthquake magnitude, m max. Pure and Applied
618 Geophysics 161(8):1655-1681
619 Kolathayar S (2021) Recent seismicity in Delhi and population exposure to seismic hazard.
620 Natural Hazards. https://doi.org/10.1007/s11069-021-04936-x
621 Kramer SL (1996) Geotechnical Earthquake Engineering. Pearson Education India
622 Maiti S, Jha SK, Garai S, Nag A, Bera AK, Paul V, Upadhaya RC, Deb SM (2017) An
623 assessment of social vulnerability to climate change among the districts of Arunachal
624 Pradesh, India. Ecological Indicators *77*:105-113.
625 Martins VN, e Silva DS, Cabral P (2012) Social vulnerability assessment to seismic risk using
626 multicriteria analysis: the case study of Vila Franca do Campo (São Miguel Island, Azores,
627 Portugal). Natural Hazards 62(2):385-404

628 Morrow BH (1999) Identifying and mapping community vulnerability. Disasters 23:1–18
629 Nath SK, Thingbaijam KKS (2012) Probabilistic seismic hazard assessment of India.
630 Seismological Research Letters 83(1):135-149
631 Nath SK, Thingbaijam KKS, Maiti SK, Nayak A (2012) Ground-motion predictions in Shillong
632 region, Northeast India. Journal of Seismology 16(3):475-488
633 NCS-MoES, National Center for Seismology, Ministry of Earth Sciences, Government of
634 India. URL: https://seismo.gov.in/MIS/riseq/earthquake (last accessed: 20 September
635 2021)
636 NDMA (2010) Development of probabilistic seismic hazard map of India; Technical Report
637 by National Disaster Management Authority, Government of India
638 Pallav K, Raghukanth STG, Singh KD (2012) Probabilistic seismic hazard estimation of
639 Manipur, India. *Journal of Geophysics and Engineering* 9(5):516-533
640 Raghukanth STG, Dash SK (2010) Deterministic seismic scenarios for Northeast India. Journal
641 of Seismology 14(2):143-167
642 Raghukanth STG, Dixit J, Dash SK (2011) Ground motion for scenario earthquakes at
643 Guwahati city. *Acta Geodaetica et Geophysica Hungarica* 46:326-346
644 Raghukanth STG, Iyengar RN (2006) Seismic hazard estimation for Mumbai city. Current
645 Science, 1486-1494
646 Ramkrishnan R, Kolathayar S, Sitharam TG (2020) Development of new ground motion
647 prediction equation for the North and Central Himalayas using recorded strong motion
648 data. Journal of Earthquake Engineering, 1-24 DOI: 10.1080/13632469.2020.1778586
649 Rydelek PA, Sacks IS (1989) Testing the completeness of earthquake catalogues and the
650 hypothesis of self-similarity. Nature 337(6204):251-253
651 Sarmah T, Das S (2018) Earthquake vulnerability assessment for RCC buildings of Guwahati
652 City using rapid visual screening. Procedia Engineering 212:214-221

653 Sharma ML, Malik S (2006) Probabilistic seismic hazard analysis and estimation of spectral
654 strong ground motion on bedrock in northeast India. In 4th International Conference on
655 Earthquake Engineering, Taipei, Taiwan, October 12-13, 2006, (Paper no. 15)
656 Sharma, S. 1996. Applied Multivariate Techniques. Wiley, Canada.
657 Siagian TH, Purhadi P, Suhartono S, Ritonga H (2014) Social vulnerability to natural hazards
658 in Indonesia: driving factors and policy implications. Natural Hazards 70(2):1603-1617
659 Sil A, Sitharam TG, Kolathayar S (2013) Probabilistic seismic hazard analysis of Tripura and
660 Mizoram states. *Natural Hazards* 68(2):1089-1108
661 Sitharam TG, Sil A (2014) Comprehensive seismic hazard assessment of Tripura and Mizoram
662 states. Journal of Earth System Science 123(4):837-857
663 Stepp JC (1972) Analysis of completeness of the earthquake sample in the Puget Sound area
664 and its effect on statistical estimates of earthquake hazard. *In Proc. of the 1st International*
665 *Conference on Microzonazion, Seattle* 2:897-910
666 USGS NEIC. US Geological Survey National Earthquake Information Center 2021, URL:
667 http://earthquake.usgs.gov/earthquakes (last accessed: 20 September 2021)
668 Stiphout TV, Zhuang J, Marsan D (2012) Seismicity declustering, Community Online
669 Resource for Statistical Seismicity Analysis, DOI: 10.5078/corssa-52382934
670 Verma RK, Kumar GK (1987) Seismicity and the nature of plate movement along the
671 Himalayan arc, Northeast India and Arakan-Yoma: a review. Tectonophysics 134(1-
672 3):153-175
673 Verma R (2018) The major drainage systems in the Northeastern region of India. In *The Indian*
674 *Rivers* (429-464). Springer, Singapore
675 Wason HR, Das R, Sharma ML (2012) Magnitude conversion problem using general
676 orthogonal regression. Geophysical Journal International 190(2):1091-1096

677 Wiemer S, Wyss M (2000) Minimum magnitude of completeness in earthquake catalogs:
678 examples from Alaska, the western United States, and Japan. Bulletin of the Seismological
679 Society of America 90(4):859-869
680 Wiemer S (2001) A software package to analyze seismicity: ZMAP. Seismological Research
681 Letters 72(3):373-382
682 Woessner J, Wiemer S (2005) Assessing the quality of earthquake catalogues: Estimating the
683 magnitude of completeness and its uncertainty. Bulletin of the Seismological Society of
684 America 95(2):684-698
685 Wood NJ, Burton CG, Cutter SL (2010) Community variations in social vulnerability to
686 Cascadia-related tsunamis in the US Pacific Northwest. Natural Hazards 52(2):369-389
687 Zhuang J, Ogata Y, Vere-Jones D (2002) Stochastic declustering of space-time earthquake
688 occurrences. Journal of the American Statistical Association, 97(458):369-380